Akira Toriumi, Lun Xu, Yuki Mori, Xuan Tian, Patrick D. Lomenzo, Halid Mulaosmanovic, Monica Materano, Thomas Mikolajick, Uwe Schroeder

Material perspectives of HfO2-based ferroelectric films for device applications

Erstveröffentlichung in / First published in:

IEEE International Electron Devices Meeting (IEDM). San Francisco, 2019. IEEE, S.15.1.2–15.1.4. ISBN 978-1-7281-4032-2

DOI: https://doi.org/10.1109/IEDM19573.2019.8993464

Final edited form was published in "IEEE International Electron Devices Meeting (IEDM). San Francisco, 2019". S.15.1.2–15.1.4.
ISBN 978-1-7281-4032-2
https://doi.org/10.1109/IEDM19573.2019.8993464

Material perspectives of HfO_2-based ferroelectric films for device applications

Akira Toriumi[1,2], Lun Xu[1], Yuki Mori[1], Xuan Tian[1], Patrick D. Lomenzo[2], Halid Mulaosmanovic[2], Monica Materano[2], Thomas Mikolajick[2], and Uwe Schroeder[2]
[1]Department of Materials Engineering, The University of Tokyo, Tokyo 113-8656, Japan
[2]NaMLab/TU-Dresden, Dresden 01187, Germany
e-mail: toriumi@material.t.u-tokyo.ac.jp

Abstract*— *Ferroelectric HfO_2 attracts a huge amount of attention not only for memory and negative capacitance, but also for programmable logic including memory-in-logic and neuromorphic applications. However, the understanding of material fundamentals still needs to be improved. This paper gives material fundamentals and new insights to this ferroelectric material for future device applications. In particular, the key role of dopants, effects of the interface on the ferroelectric phase, and a detailed discussion of the switching kinetics are of central focus. Based on material properties newly obtained, we discuss opportunities of ferroelectric HfO_2 for device applications.

INTRODUCTION

Since the first publication on ferroelectric HfO_2, it has been reported that various dopants can stabilize the ferroelectric (FE) properties in HfO_2 films [1-5]. Although oxygen vacancies (Vo's) formed during processing are often discussed as a possible origin for FE orthorhombic phase formation of polymorphic HfO_2, it has not been clearly understood how dopants and other process conditions induce the FE phase in HfO_2. And, it was reported that even un-doped HfO_2 exhibited FE behaviors [6-8]. Besides, we previously reported an impact of thermal annealing transient on the resultant HfO_2 phase. A significant effect of the ramp-down speed on the structural phase stabilization of the high-temperature phase was demonstrated [9]. Since it is inferred empirically that the FE phase in HfO_2 is formed at the boundary between monoclinic and tetragonal phases [10], the FE-phase formation should also be sensitive to the post deposition anneal (PDA) transients. Furthermore, the polarization switching kinetics in FE is critically important for applications in terms of speed and power supply voltage. Therefore, the objective of this work is to clarify **(i)** key roles of doping as well as **(ii)** of interface electrode in FE phase HfO_2 formation. Furthermore, **(iii)** coercive field (*Ec*) and the polarization switching kinetics are discussed. Finally, the power supply voltage in FE-HfO_2 devices is discussed from device application viewpoints. Introduction

KEY ROLE OF DOPANTS IN FE-HfO_2

The impact of various dopants on the FE-phase formation was studied systematically (**Fig. 1**) [10]. More recently, a universal relation of the remanent polarization (P_r) versus normalized dopant concentration in HfO_2 has been characterized (**Fig. 2**), and a normalization factor α was determined (see the caption for the normalization) as a function of the ionic radius, as shown in **Fig. 3**. A clear difference is visible for tetravalent dopants like Si, Ge or Zr in contrast to trivalent dopants (e.g. Y or Sc). Both are expected to be positioned in Hf sites within HfO_2 unit cell. Trivalent dopants are expected to generate Vo's in HfO_2 to compensate the charge imbalance. Results distinguish the simple Vo effect from tetravalent dopant effect on FE phase formation. Accordingly, we cannot say simply everything comes from Vo in HfO_2, but should take account of the bonding orbital-induced internal stress/strain. For the device fabrication viewpoint, the dopant size impacts the HfO_2 crystallization temperature. Hence, dopants with an atomic radius close to Hf need to be selected for a low temperature e.g. capacitor application and other dopants for devices with high thermal budget as in gate-first FE-FETs.

Next, effects of PDA are discussed to get more insights to the impact of Vo on FE phase formation. Y-doped HfO_2 was deposited on TiN electrode. Before top electrode deposition, different PDAs were carried out in N_2 using a rapid-thermal-annealing (RTA) furnace, having a sample stage designed with a very small heat capacity. The temperature was monitored by the thermocouple directly touching the sample. The peak temperature was set to be 600°C. During PDA, both the ramp-up time up to 600°C and ramp-down time back to 200°C could be varied. Samples were characterized by XRD and polarization versus voltage (P-V) hysteresis. The PDA process can be divided into a ramp-up, holding and ramp-down phases. Since as-deposited films are initially amorphous, a tetragonal HfO_2 should be formed at the initial nucleation step. Therefore, the ramp-up time (τ↑) was set to be rather fast in this study (2.5 sec/100K). Since the holding-time should be related to the growth period or the phase transition process, it was fixed to 10 s. The up and down rate τ↑↓ was defined by (sec/100°C).

Fig. 4(a) and **(b)** show XRD patterns for un-doped HfO_2 and 1.7 % (Y/Hf ratio) Y-HfO_2 as a function of τ↓ in PDA. It is merely dependent on τ↓ whether un-doped HfO_2 shows FE or not (data not shown). In case of (b) 1.7 % Y-HfO_2, only a slight structural phase transformation is seen in a long τ↓. In any τ↓, FE features were clearly observed. To verify this trend, $2P_r$ is plotted as a function of the monoclinic phase portion r_m in **Fig. 5**, with r_m derived from the XRD peak intensity at 2θ~30° as

$$r_m = \frac{I_{m(-111)} + I_{m(111)}}{I_{m(-111)} + I_{m(111)} + I_{o/t/c(111)}}.$$

P_r is simply determined by r_m irrespective of doping concentration or τ↓. In addition, $2P_r$ can be plotted as a function of τ↓ for three HfO_2 films with different Y content (un-doped, 1.0 %, and 1.7 % Y/Hf ratio). With the increase in Y%, less dependence of P_r on τ↓ is observed in **Fig. 6**. More interestingly, an extrapolated value of P_r to τ↓=0 seems to be a given value irrespective of Y%. Namely, P_r value is the same for different doped case, if the perfect quenching could be carried out. With the increase in τ↓, P_r in Y:1.7 % HfO_2 does not change in the experimental time range, while that in un-doped case is significantly degraded. This fact suggests that amount of Vo's in HfO_2 at 600°C is the same both doped and un-doped HfO_2 films. The dopant, Y in the present case, just stabilizes the FE phase structure in PDA even with a long τ↓, while un-doped HfO_2 cannot maintain FE phase and relaxes to monoclinic one in a long τ↓ at room temperature (**Fig. 7**). **Fig. 8** shows the energy landscape in which the energy barrier in the structural transformation from FE to monoclinic phase is decreased in the long τ↓. The impact of dopants and quenching is indicated by the red dotted line. Vo's in undoped HfO_2 can

Final edited form was published in "IEEE International Electron Devices Meeting (IEDM). San Francisco, 2019". S.15.1.2–15.1.4.
ISBN 978-1-7281-4032-2
https://doi.org/10.1109/IEDM19573.2019.8993464

diffuse and interact with the film, causing a structural relaxation, while dopants are at a stable position within HfO_2 and stabilizing Vo. Thus, a dopant serves as the Vo stabilizer.

INTERFACIAL EFFECTS ON FE-HfO_2

It is naturally expected that electrode may affect the FE formation of HfO_2. The bottom and top electrodes are important for FE-capacitor and for FE-FET applications, respectively. **Fig. 9** gives an example of bottom electrode effects (Pt, TiN, and p^+-Ge) on HfO_2 with top Au. In this study, un-doped HfO_2 films were used to highlight possible electrode effects. No FE properties are observed on Pt, while clear FE on TiN and p^+-Ge. In addition, top electrode difference between nitrides and oxides on structural phase of HfO_2 were compared in XRD. There was very little difference of HfO_2 phase in PMA among Al_2O_3, TiO_2 and SiO_2, and AlN, TiN and TaN (data not shown), in spite of a big difference from HfO_2 with no top-layer in PDA. Hence, a chemical reaction at the top interface is primary not a matter, but that suppressions of the structural relaxation and the out- or in-diffusion of oxygen in PMA are important for keeping FE properties stable.

For particular application such as ferroelectric tunnel junctions (FTJs), the electrode selection is essential. HfO_2 on highly-doped Ge shows clear FE properties (Fig. 9), and no interlayer is detected in XTEM (**Fig. 10**). In case of Si electrode, SiO_x interlayer is inevitably formed due to its thermodynamic stability. This means a metal/FE-HfO_2/p^+-Ge may be the most viable choice for FTJs. In fact, very low voltage FTJ operation was demonstrated [11], as shown in **Fig. 11**. The on/off ratio of 10 at V_{read}=0.2 V and V_{write}=1.6 V in 2.7-nm-thick FE-HfO_2 is very promising. The electrode on HfO_2 should be selected for applications.

COERCIVE FIELD AND POLARIZATION SWITCHING KINETICS IN FE-HfO_2

For most FE-HfO_2 based devices currently in discussion: FE capacitors, FE-FETs including NC-FETs, and FTJs, a detailed understanding of FE-switching is mandatory. The most significant factor is the coercive field (E_C).

First, E_C is plotted for different dopants in HfO_2, again as a function of the monoclinic portion in **Fig. 12**. Higher E_C values are present for trivalent dopants in contrast to the tetravalent dopants like Ge, Si and Zr. This fact makes tetravalent dopants more favorable for a device application. In addition, it is interesting to remember that those doped-HfO_2 films exhibit anti-ferroelectric properties.

Next, E_C is plotted for different thickness in Ge-doped HfO_2 in contrast to PZT (as reported) in **Fig. 13**. At a physical thickness of 10 nm, E_C of HfO_2 is about a factor of 10 higher than that of PZT, resulting in a better retention behavior of HfO_2, but also a higher field necessary for polarization reversal. Here, an absolute value of E_C is reconsidered. According to the simple Landau formula, E_C is described as [14],

$$E_C = \pm \frac{1}{3\sqrt{3}} \left(\frac{P}{k\varepsilon_0} \right)_{E=0}$$

By assuming Ps~30 μC/cm^2 and k~30, E_C is roughly 2 MV/cm, which is very reasonable for the experimental result. Since E_C value generally disagrees with the Landau theory, the sidewise domain growth was proposed and well fitted to experiments. In addition, note that a dramatic difference of the thickness (d) dependence is observed between HfO_2 and PZT. In HfO_2, rather no thickness dependence of E_C [6, 12], while $E_C \sim d^{-2/3}$ has been often reported in PZT [13]. This flat trend in HfO_2 has also been reported in literatures [6, 12]. Above results strongly suggest that the switching kinetics in HfO_2 may not be described by the domain growth model (KAI:Kolmogorov-Avrami-Ishibashi model) [15]. Hence, another one, NLS (nucleation-limited-switching) model [16] is a candidate. **Fig. 14** schematically compares NLS one, in which the lateral domain growth (sidewise growth) is not relevant, with KAI model. Here, to further investigate the switching kinetics, the pulse *I-V* measurement for characterizing the switching kinetics was carried out by changing the frequency and amplitude [17]. **Fig. 15** represents the experimental results which are on a straight line in the semi-log plot both for HfO_2 and PZT. The results can be expressed as follows.

$$\frac{1}{\tau} = \frac{1}{\tau_0} \exp\left(-\frac{\gamma}{{E_c}^2} \right) \quad \gamma: constant.$$

It means that for both FE-HfO_2 and thin poly-PZT, NLS behavior can be strongly suggested [18]. From the result in Fig. 15, a supply voltage of ~2.6 V is necessary for HfO_2 to switch ~90% of the FE domains in 10 ns. For longer switching times, lower voltages can be utilized. Thus, NLS and high E_C in FE-HfO_2, are for and against the fast switching under a power supply voltage, respectively. NLS also implies that a voltage below E_C would finally lead to a stochastic switching event in scaled devices [19]. This is beneficial for neuromorphic FE-FET applications, while it needs to be taken into account for read/write disturbs in a memory array.

Almost no interlayers are present in FE capacitors and the supply voltages below 3V are possible. On the other hand, for MIS or SIS based FE-FETs, supply voltages should be enhanced due to an additional voltage drop at the interlayer(s). **Fig. 16(a)** shows an allowable voltage area for FE switching below the breakdown field (E_{BD}) and above E_C in case of no interlayer, and **(b)** displays an overview of reported and measured switching voltages for FE-FETs. Thinner IL is obviously more needed for a low power supply voltage operation. Thus, in FE-FET applications, the interlayer engineering is especially a key to the low power operation, in addition to FE properties.

CONCLUSION

Material fundamentals of FE-HfO_2 and polarization switching kinetics in FE-HfO_2-based devices have been discussed. FE-HfO_2 is the most promising for new memory and logic applications. However, high Ec is intrinsically challenging to high-speed operation under a low supply voltage, while NLS kinetics is favorable. Thus, the dopant selection should be made in terms of lowering Ec. On the other hand, the minor-loop application in FE properties will be attractive for neuromorphic applications, in addition to the fact that novel FE memory technologies are charming toward the future.

ACKNOWLEDGMENT

This work was partly supported by JST-CREST (JPMJCR14F2). AT is grateful to the TU-Dresden Fellowship for staying at NaMLab in 2019 summer.

References

[1] T. S. Böscke et al., APL **99**, 102903 (2011). [2] J. Müller et al., JAP **110**, 114113 (2011). [3] S. Mueller et al., Adv. Func. Mat. **22**, 2412 (2012). [4] J. Müller et al., Nano Lett. **12**, 4318 (2012). [5] L. Xu et al., APEX **9**, 091501 (2016). [6] T. Olsen et al., APL **101**, 082905 (2012). [7] T. Nishimura et al., JJAP **55**, 08PB01 (2016). [8] T. Mittmann et al., Adv. Mat. Int. **6**, 1900042 (2019). [9] Y. Nakajima et al., VLSI Tech. Symp. 84 (2011). [10] L. Xu et al., JAP **122**, 124104 (2017). [11] X. Tian et al., SSDM, 197 (2018). [12] S. Migita et al., JJAP **57**, 04FB01 (2018) [13] M. Daber et al., J. Phys. Cond. Mat., 14L393 (2003). [14] V. Fridkin and S. Ducharme, Phys. Solid State **43**, 1320 (2001). [15] Y. Ishibashi, JJAP **31**, 2822 (1992). [16] A. K. Tagantsev et al., PRB **66**, 214109 (2002). [17] D. Jung et al., Integ. Ferro. **48**, 59 (2002), S-M Nam et al., JJAP **42**, L1519 (2003). [18] N. Gong et al., APL 112, 262903 (2018). [19] H. Mulaosmanovic et al., ACS Appl. Mat&Int. **10**, 23997 (2018).

Final edited form was published in "IEEE International Electron Devices Meeting (IEDM). San Francisco, 2019". S.15.1.2–15.1.4.
ISBN 978-1-7281-4032-2
https://doi.org/10.1109/IEDM19573.2019.8993464

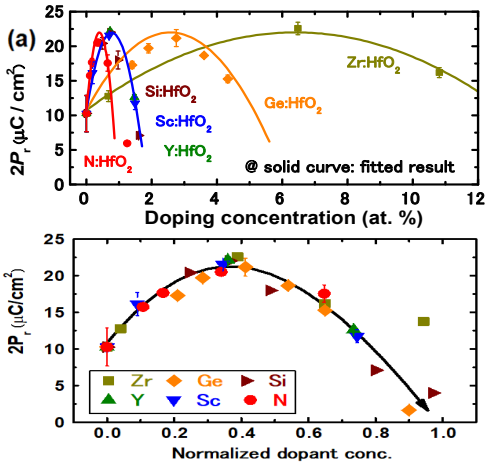

Fig.1 2*Pr* as a function of the concentration of each dopant, in which it should be noted the concentration is taken for the total atom number. Although this result has been reported in ref. 10, it is put here because of the starting point of this work.

Fig.2 2*Pr* as a function of normalized concentration to fit a universal parabolic line. The normalization factor, α, for the dopant concentration is fixed to be 0.5 for Sc, because Sc^{3+} has almost the same ionic radius as Hf^{4+}.

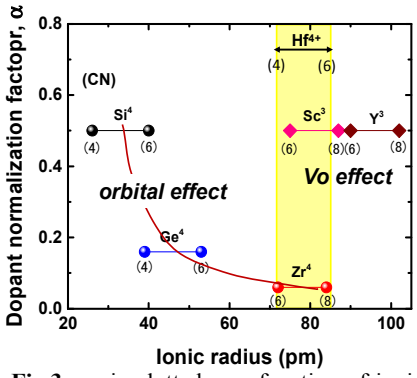

Fig.3 α is plotted as a function of ionic radius. Two kinds of trends are seen for FE stabilization. The number in (*n*) represents the coordination number, *n*, of each atom.

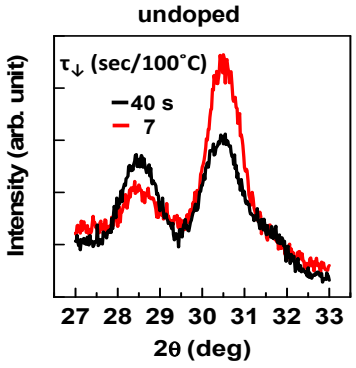

Fig.4(a) XRD patterns in un-doped HfO_2 films with two typical τ↓. In the un-doped case, the peak intensity changes dramatically by changing τ↓ from 7 (red) to 40 s (black).

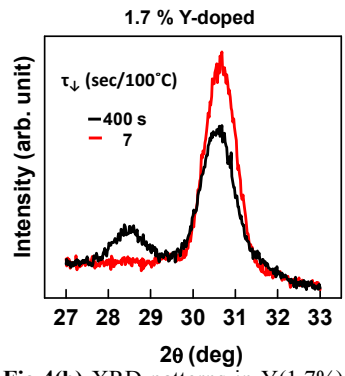

Fig.4(b) XRD patterns in Y(1.7%)-doped HfO_2 samples with two typical τ↓. The monoclinic phase gradually but slowly increases with the increase in τ↓. Note that τ↓(black) is *10*x longer than that in undoped case.

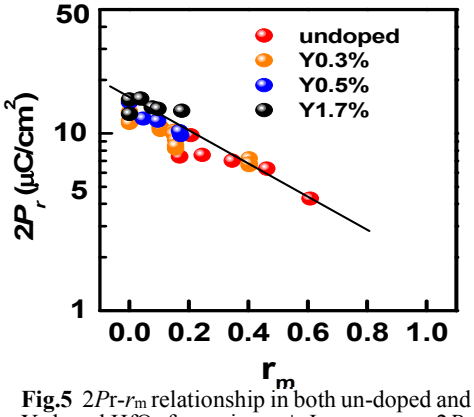

Fig.5 2*Pr*-r_m relationship in both un-doped and Y-doped HfO_2 for various τ↓. In any cases, 2*Pr* is well described by r_m. Although this trend is not physically clarified yet, it empirically holds good for samples evaluated so far. (1-r_m) corresponds to the symmetric phase, which includes orthorhombic phase.

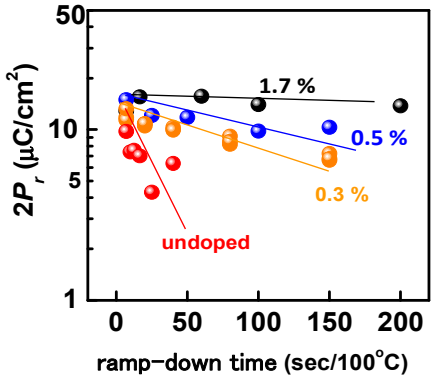

Fig.6 2*Pr* as a function of τ↓ defined by sec/100°C for three kinds of Y-doped and un-doped HfO_2. Note that extrapolated 2*Pr* values converge onto one point irrespective of dopant concentration including un-doped case. This fact indicates that dopant can stabilize the FE phase structure, which is quenched by quick ramp-down process as well.

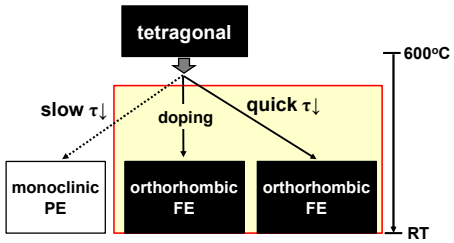

Fig.7 Schematic view of structural phase transformation in HfO_2 under the ramp-down process in PDA. Tetragonal phase at 600°C is not formed by the doping but by intrinsic properties in thin HfO_2. Since the tetragonal-monoclinic transformation is associated with a shear deformation, the dopant suppresses the deformation with the help of Vo or bonding-orbital force effect.

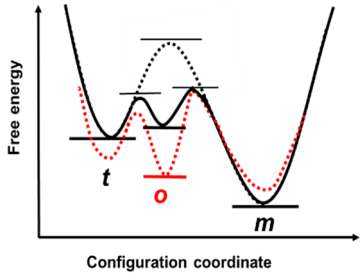

Fig.8 Schematically depicted energy landscape in structural phase transformation process of HfO_2. A solid-black line denotes un-doped HfO_2 case with the normal PDA, while in red-broken one shows doped or quick ramp-down case. A broken-black line shows the classical picture of the transition from tetragonal to monoclinic. It is inferred that FE-phase is at metastable state with a finite energy barrier from FE- to ground state.

Final edited form was published in "IEEE International Electron Devices Meeting (IEDM). San Francisco, 2019". S.15.1.2–15.1.4.
ISBN 978-1-7281-4032-2
https://doi.org/10.1109/IEDM19573.2019.8993464

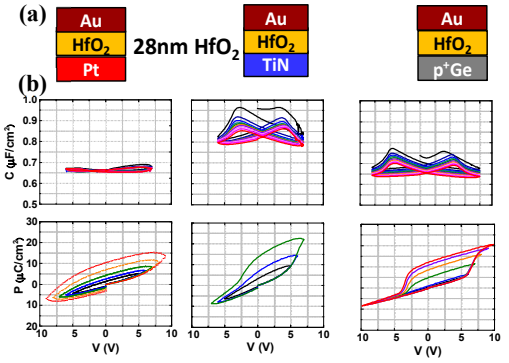

Fig.9 (a) Schematic views s of three kinds of bottom electrode structures (Pt, TiN and p^+-Ge) in un-doped HfO_2. **(b)** C-V and P-V characteristics in each stack. PDA was at 600°C. Repetitive C-V and V-swing increase in P-V are demonstrated.

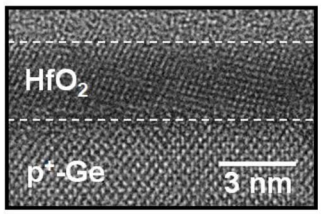

Fig.10 X-TEM image of p^+-Ge/HfO_2 after PDA at 600°C. No interlayer is formed on p^+-Ge. All the results in Fig. 1 was obtained on p^+-Ge. In case of Si, SiO_x interlayer is inevitably formed. This will be a big advantage of Ge devices

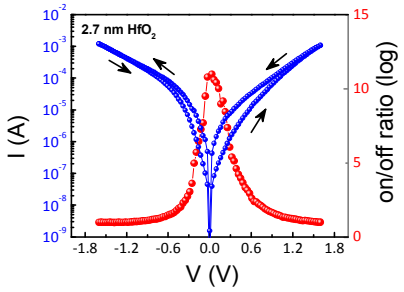

Fig.11 I-V characteristics in TiN/Y-HfO_2/p^+-Ge junction. HfO_2 thickness was 2.7 nm and P_r was ~4 μC/cm². 1.6 V writing, 0.2 V reading proved the on/off ratio ~10. No area dependence was observed. In Ge electrode, a big difference of electron density between top and bottom electrodes is very advantageous for FTJs, in addition to no interlayer formation.

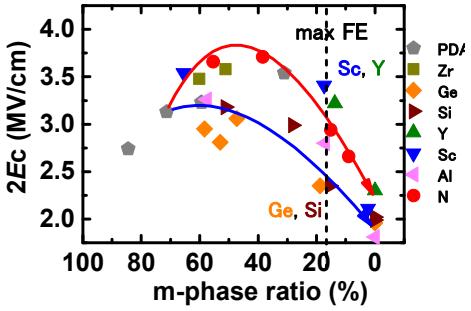

Fig. 12 2*Ec* is plotted as a function of r_m x100 % for many dopants. Two trends are seen. The results may suggest that one (red line) is Vo-driven FE, while the other (blue line) is bonding orbital-driven one.

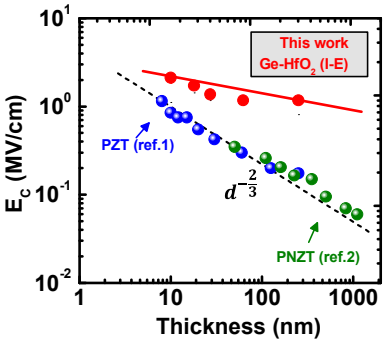

Fig. 13 Thickness dependence of *Ec* both for Ge-doped HfO_2 and PZT (ref.1, *N. Pertsev et al., APL* ***83****, 3356 (2003);* ref.2,*C. Bjormander et al., APL* ***64****, 2493 (1994)*). *Ec* in PZT is on a line with the power law of oxide thickness (*d*), while E_C in HfO_2 looks rather flat.

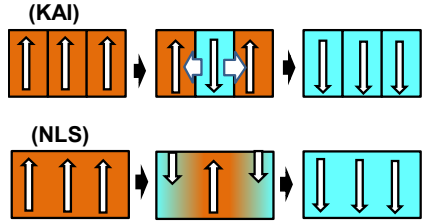

Fig. 14 Two kinds of polarization switching model. The upper is KAI model, in which the lateral domain-wall growth eventually changes the polarization direction through the film, while the lower is NLS one, in which the domain growth is not involved. In KAI model, a rather long time to switch the polarization is a matter of concern.

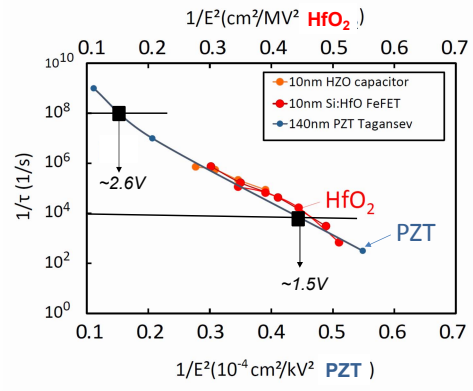

Fig. 15 Polarization switching analysis using the pulse *I-V* measurement for two kinds of HfO_2 samples, and poly-PZT. Experimental details are found in ref. [17]. A linear relationship between $1/\tau$ and $1/E^2$ suggests that NLS is a proper model, in which τ and *E* are the pulse width and applied electric field, respectively. Note a unit difference of the horizontal axis *E* between HfO_2 and poly-PZT (a scale difference between the top and bottom axes). From this trend, ~2.6 V and ~1.5 V are needed for 10 ns and 100 μs polarization switching.

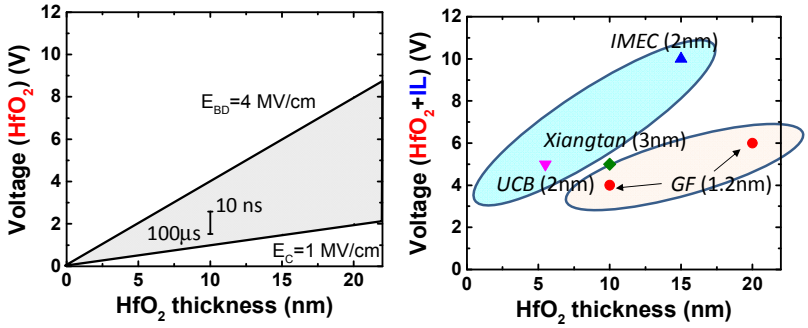

Fig.16 Thickness-voltage relationship for HfO_2 FE-FETs (for 1Tr memory). **(a)** Two fixed oxide electric field lines (1and 4 MV/cm) are shown for E_C and E_{BD}. Voltage applied on HfO_2 should be in this triangle area. Reliability, memory window and actual voltage swing are estimated in this figure. 2.6 V (10 ns) and 1.5 V(100 μs) operating points from Fig. 15 are shown in the plot. **(b)** Data points are from literatures, which include the finite interlayers (IL). (*GF IEDM 2015, UCB EDL 2017, IMEC IEDM 2018, Xiangtan JEDS 2019*). (#) denotes IL thickness. Thinner IL allows a lower total voltage, while thicker HfO_2 is better for achieving a larger memory window. Thus, when the power supply voltage is fixed to be low, the interlayer engineering is critical for keeping the high-speed polarization switching.